

# CMB and foregrounds in WMAP first year data.

G. Patanchon<sup>1</sup>, J.-F. Cardoso<sup>2</sup>, J. Delabrouille<sup>3</sup>, P. Vielva<sup>3</sup>

<sup>1</sup> *Department of Physics & Astronomy, University of British Columbia, 6224 Agricultural Road, Vancouver, BC V6T 1Z1, Canada*

<sup>2</sup> *CNRS/ENST — 46, rue Barrault, 75634 Paris, France*

<sup>3</sup> *PCC — Collège de France, 11, place Marcelin Berthelot, F-75231 Paris, France*

Accepted ??, Received ??; in original form ??

## ABSTRACT

We perform a blind multi-component analysis of the WMAP 1 year foreground cleaned maps using SMICA (Spectral Matching Independent Component Analysis). We provide a new estimate of the CMB power spectrum as well as the amplitude of the CMB anisotropies across frequency channels. We show that the CMB anisotropies are compatible with temperature fluctuations as expected from the standard paradigm. The analysis also allows us to identify and separate a weak residual galactic emission present significantly in the Q-band outside of the Kp2 mask limits, and mainly concentrated at low galactic latitudes. We produce a map of this residual component by Wiener filtering using estimated parameters. The level of contamination of CMB data by this component is compatible with the WMAP team estimation of foreground residual contamination. In addition, the multi-component analysis allows us to estimate jointly the power spectrum of unresolved point source emission.

**Key words:** Cosmic microwave background – Cosmology: observations – Methods: data analysis

## 1 INTRODUCTION

The Cosmic Microwave Background (CMB) is one of the most powerful probe of modern cosmology. The shape of the spatial power spectrum of the small temperature fluctuations depend on the cosmological parameters describing, in the frame of the standard model, the matter content, the geometry, and the evolution of the Universe (Jungman et al. 1996). Since the first detection of CMB anisotropies by the COBE satellite in 1992 (Smoot et al. 1992), several ground-based and balloon-borne experiments have provided an accurate estimate of the power spectrum on a large range of angular scales. The recent WMAP mission (Bennett et al. 2003a), after one year of data acquisition, provided measurements of the power spectrum with unprecedented accuracy.

Measuring the CMB power spectrum is a difficult task. It requires a good characterization of noise contribution in the observations, as well as the subtraction of foreground astrophysical emission present at millimeter wavelengths (Bouchet & Gispert 1999). Both noise and foreground emissions can significantly bias CMB power spectrum estimates if not well accounted for.

The WMAP data is the best presently available observation of the sky in the 20-90 GHz range. A careful separation of CMB from foregrounds, however, is required in order to make the best out of these observations. In particular, isolating CMB from foregrounds is of extreme importance

for measuring accurately the angular power spectrum  $C(\ell)$  of CMB anisotropies and for cosmological interpretation.

The approach of the WMAP collaboration consists in cleaning observations from foreground contaminations for performing a CMB power spectrum estimation on the cleaned maps. More specifically, galactic foregrounds are subtracted using templates obtained from external data sets. In addition, strong known extra-galactic point sources, as well as the region of the galactic plane, are masked prior to the analysis. The CMB spectrum is estimated using a weighted average of the cross-power spectra of cleaned observation maps in the Q, V and W channels (Hinshaw et al. 2003). This avoids biases due to detector noise, assuming that the noise of different detectors is uncorrelated. This estimated spectrum is corrected for residual point source contamination by subtracting an estimate of the contribution of point sources in the cross power spectra. The level of residual galactic contaminations is estimated by cross-correlating the maps with foreground templates.

A multi-component approach of CMB spectral estimation has been proposed by Delabrouille, Cardoso, Patanchon (2003). Additional publications on the subject give variants and details (Cardoso et al. 2002; Patanchon et al. 2003). The method, called SMICA (Spectral Matching Independent Component Analysis), is based on matching the cross- and auto-power spectra of the observed maps to a parametric model

described by the power spectra of all the astrophysical components, their relative amplitudes in the different channels, and the noise power spectra. It is a very flexible approach: depending on available knowledge, most of the parameters may be either estimated from the data or kept at fixed values. In particular, emission laws for all or some of the components can be estimated.

There are several benefits to using SMICA in CMB analysis.

First, SMICA is equivalent to a maximum likelihood estimation of the CMB power spectrum if the observed maps are a linear mixture of Gaussian stationary components and noise. Therefore, if there are no foregrounds but only Gaussian CMB and noise, SMICA is expected to outperform quadratic estimates.

Secondly, SMICA allows to estimate jointly the spatial power spectra *and* the amplitude of components in each channel (which are related to emission laws of components as well as calibration coefficients). In particular, the application on WMAP data allows us to check the following strong prediction of the standard model: CMB anisotropy should have a spectral emission law given, to first order, by a derivative (with respect to the temperature) of the blackbody law. Fixsen (2003) has measured the CMB anisotropy contribution in the COBE FIRAS data by looking for the WMAP anisotropy template in FIRAS. The author shows the compatibility of CMB anisotropy at large angular scales ( $> 5^\circ$ ) with temperature fluctuations in the Wien part of the spectrum. Our blind estimation of the component emission laws provides us with a unique tool for extending this result to frequencies covered by WMAP and to all measured angular scales (including the first acoustic peak) with a remarkable precision as shown below.

Finally, if there are foreground contributions in the observations, SMICA is designed to detect them and allows their separation. It permits indeed to jointly estimate power spectra of multiple components in the data, *to assess the significance of components*, and eventually to separate the effect of all the emissions.

In this paper, we investigate the existence of residual foreground emission in foreground-cleaned WMAP data. In particular, residual galactic emission resulting from an error in the subtraction of galactic templates can be present in the published maps. Such residuals may exist if external templates of galactic emissions, extrapolated using a physical model to WMAP frequencies, are not quite representative of the actual galactic components. Multi-component analysis with SMICA allows to check for the existence of such a residual, and to quantify the level of contamination if any, without prior information on its power spectrum or on its amplitude across channels.

In addition, the WMAP collaboration has shown that unresolved point source emissions have a non-negligible contribution to the data (Hinshaw et al. 2003; Komatsu et al. 2003). This result has been independently confirmed by Huffenberger, Seljak, Makarov (2004). As will be shown, SMICA also yields a coarse estimate the level of point source emission in WMAP data.

The paper is organized as follow: section 2 introduces the data used for the analysis, the simulations performed in order to check our results and the model of the WMAP ob-

servations for SMICA. The method is described in section 3. Section 4 presents the different results. Finally, conclusions are provided in section 5

## 2 DATA

### 2.1 WMAP data and input maps for SMICA

The WMAP space probe, launched by NASA in 2001, is a large telescope for imaging the total emission of the sky at 5 different wavelengths (or frequency channels), with a resolution ranging from about 0.2 degrees to 0.9 degrees (limited by diffraction), and with full sky coverage (Bennett et al. 2003a).

The data taken by WMAP has been made available to the scientific community after one year of proprietary period, and is freely available on a dedicated NASA CMB web site.<sup>1</sup> The data consists in a set of 10 maps obtained by different detector pairs: four maps at 3.2 mm (W band at 94 GHz), two at each 4.9 mm and 7.3 mm (V band at 61 GHz and Q band at 41 GHz), and one at 9.1 mm and at 13.0 mm (Ka band at 33 GHz and K band at 23 GHz). The data is provided in the HEALPix pixellisation format of the sphere<sup>2</sup> (Górski, Hivon, Wandelt 1998). Foreground cleaned versions of the Q, V and W-band maps are also available. These maps have been used in the generation of the WMAP first-year CMB power spectrum by the WMAP team. The Galactic foreground signal, consisting of synchrotron, free-free, and dust emission, was removed using the 3-band, 5-parameter template fitting method described in Bennett et al. (2003b). Galactic templates come from external data sets: the 408 MHz synchrotron map (Haslam et al. 1982), the predicted dust emission at 94 GHz using the FDS model (Finkbeiner, Davis & Schlegel 1999), composite H $\alpha$  map (Finkbeiner 2003) and the galactic reddening E(B-V) (Schlegel, Finkbeiner & Davis 1998).

For our analysis, we use the eight individual foreground cleaned maps. We partially correct the maps from beam smoothing effects, so that every map gets the effective resolution of a reference map (we choose W3). We simply multiply the coefficients of the spherical harmonic decomposition by the inverse of beam transfer function ratio.

We consider two different sets of maps corresponding to different masking. For the first set (hereafter map set I), we apply the Kp2 galactic mask provided by the WMAP collaboration, canceling about 15% of the pixels. For the second set (hereafter map set II), we mask the pixels corresponding to galactic latitudes lower than 40 degrees. For both sets, we mask the strongest point sources using the mask provided by the WMAP team. In all cases masks are apodised for a smooth transition between 0 and 1 on a scale of 30 arcmin.

The prior correction of beam smoothing effects permits the application of SMICA using directly the pseudo cross- and auto-power spectra of observation (computed from partially covered maps). The true component power spectra can be obtained from these pseudo power spectra afterwards.

<sup>1</sup> <http://lambda.gsfc.nasa.gov/>

<sup>2</sup> <http://www.eso.org/science/healpix/>

## 2.2 Simulations

In order to validate the method, assess error bars on the estimated parameters, and check for systematic errors in the analysis, we have generated 100 full-sky simulations of the WMAP observed maps with 6.5 arcmin pixels (HEALPix  $n_{\text{side}} = 512$ ). Each set of simulations consists in 8 maps reproducing the observations in the Q, V and W bands. Maps contain synthetic CMB anisotropies degraded to the resolution of the detectors, assuming a symmetric beam pattern and using the transfer function published by WMAP. They contain anisotropic white noise at the expected level. CMB anisotropies are generated using the CMBFAST software (Zaldarriaga & Seljak 2000) with current ‘concordance’ cosmological parameters (Spergel et al. 2003). The simulated maps are partially deconvolved and the same mask as used for real data is applied.

No measurable bias has been observed in simulations. Error bars on all parameters (CMB power spectrum as well as mixing parameters) obtained from the dispersion over 100 independent simulations have been found to be in very good agreement (precision better than 10%) with the closed form expression of eq. (13), validating the use of the latter for final error bar estimates.

## 2.3 Model of the WMAP observations

The sky emission at WMAP frequencies is well described to first order by a linear superposition of the emissions of a few processes: CMB anisotropies, galactic foregrounds (synchrotron, dust, free-free. . .), point source emissions and Sunyaev Zel’dovich (SZ) effect. After subtraction of the galactic foreground templates and masking, the WMAP data between 40 and 94 GHz can be modeled as noisy linear mixtures of CMB anisotropies, unresolved point sources and possibly small residual galactic emissions (no significant SZ effect is expected to be present in WMAP observations (Bennett et al. 2003b), and Huffenberger, Seljak, Makarov (2004) found no evidence of SZ effect using a multi-frequency approach). We assume that the emission laws of components are independent of the position  $(\theta, \phi)$  on the sky. Although this is only an approximation, it holds exactly for the CMB and for galactic residuals which are significant at one frequency only. Thus, observation  $i$  is modeled as

$$x_i(\theta, \phi) = \sum_{c=1}^{N_c} A_{ic} s_c(\theta, \phi) + n_i(\theta, \phi) \quad (1)$$

where  $s_c$  is the spatial distribution of component  $c$ ,  $n_i$  is the noise of observation  $i$  and  $A_{ic}$  is the amplitude of component  $c$  in map  $i$  given by

$$A_{ic} = \int w_i(\nu) g_c(\nu) d\nu \quad (2)$$

where  $w_i$  is the spectral band of detector  $i$  and  $g_c(\nu)$  is the emission law of component  $c$ . In matrix-vector format, model (1) reads

$$x(\theta, \phi) = A s(\theta, \phi) + n(\theta, \phi) \quad (3)$$

with an  $N_d \times N_c$  mixing matrix  $A$ .

This simple model does not reflect the fact that resolution depends on the frequency band. In our analysis, this

effect, as well as the impact of the masks, is accounted for in the spectral domain: see section (3.4), for a sketch of the correction of beam and coverage effects.

On the statistical side, we shall assume statistical independence between components, between the noise contaminations of different detectors, and between the latter and all the components.

The standard model of cosmology predicts that CMB anisotropies are small temperature fluctuations of a pure blackbody spectrum. A first order expansion around  $T = 2.726$  K gives:

$$g_{\text{CMB}}(\nu) \propto \left[ \frac{\partial B_\nu(T)}{\partial T} \right]_{T=2.726 \text{ K}} \quad (4)$$

where  $B_\nu(T)$  is the Planck law for the emission of a blackbody at temperature  $T$ .

Whereas the assumption that  $A_{ic}$  does not depend on the position is a good approximation to first order for galactic components, it is not the case for point source emissions. Nevertheless, since the brightest point sources are masked and since the frequency dependence of most of contributing radio sources belong to the flat population, their emission law can be roughly described as:

$$g_{\text{PS}}(\nu) \propto \left( \frac{\nu}{\nu_0} \right)^\beta \quad (5)$$

with  $\beta \approx -2$  (Toffolatti et al. 1998). Note that unresolved point sources in the WMAP data have already been reported at a very low level (Hinshaw et al. 2003).

## 2.4 Spectral statistics

The spectra and cross-spectra at frequency  $\ell$  of  $x(\theta, \phi)$  (considered as an isotropic  $N_d$ -dimensional random field on the sphere) is the  $N_d \times N_d$  spectral matrix  $R(\ell)$

$$R(\ell) = \langle x(\ell, m) x(\ell, m)^\dagger \rangle \quad (6)$$

where  $\langle \cdot \rangle$  denotes an ensemble average, superscript  $\dagger$  denotes transposition and the  $x(\ell, m)$  are the coefficients of the field on the basis of real spherical harmonics. This average value is independent of  $m$  because of isotropy.

In the linear model of eq. (3), independence between components and noise implies that

$$R(\ell) = AC(\ell)A^\dagger + N(\ell) \quad (7)$$

where  $C(\ell)$  and  $N(\ell)$  are the spectral matrices for the components and the noise respectively. They are both diagonal matrices as a consequence of the independence assumption between components and between noise contaminations.

In practice, spectral matrices are estimated by averaging over frequency bins. Typically, one considers  $Q$  frequency bins with the  $q$ -th bin ( $1 \leq q \leq Q$ ) containing all harmonic modes  $(\ell, m)$  such that  $\ell_{\min}(q) \leq \ell \leq \ell_{\max}(q)$ . If  $n_q = \sum_{\ell=\ell_{\min}(q)}^{\ell_{\max}(q)} (2\ell + 1)$  denotes the number of modes in the  $q$ th harmonic bin, then the empirical spectral matrix

$$\widehat{R}_q = \frac{1}{n_q} \sum_{\ell=\ell_{\min}(q)}^{\ell_{\max}(q)} \sum_{m=-\ell}^{\ell} x(\ell, m) x(\ell, m)^\dagger \quad (8)$$

is the natural estimate of the average spectral matrix

$$R_q = \frac{1}{n_q} \sum_{\ell=\ell_{\min}(q)}^{\ell_{\max}(q)} (2\ell+1)R(\ell). \quad (9)$$

The latter inherits its structure from (7) as:

$$R_q = AC_qA^t + N_q \quad (10)$$

with average spectral matrices  $C_q$  and  $N_q$  related to  $C(\ell)$  and  $N(\ell)$  as in definition (9).

### 3 SPECTRAL ESTIMATION AND COMPONENT SEPARATION WITH SMICA

The goal of our analysis is to identify and separate the components present in WMAP maps, to evaluate the amplitude of CMB anisotropies as a function of observation wavelength (as given by the corresponding column of  $A$ ), and to provide accurate estimates for power spectra of the CMB and other components. This section briefly describes a multi-detector, multi-component analysis method. It is a maximum likelihood method based on a model of statistically independent components. Since it can be understood as a spectral matching technique, it is dubbed ‘‘SMICA’’, standing for ‘‘spectral matching independent component analysis’’. More details on SMICA can be found in Delabrouille, Cardoso, Patanchon (2003).

#### 3.1 Spectral matching

The SMICA analysis technique consists in minimizing a measure of the mismatch between the empirical covariance matrices  $\hat{R}_q$  and their model counterparts  $R_q$ . Minimization is conducted with respect to any relevant set of parameters describing the covariance matrices  $R_q$ . The maximal parameter set is made of: the entries of the mixing matrix  $A$ , the average power  $[C_q]_{cc}$  of the  $c$ -th component in the  $q$ -th bin, and the average power  $[N_q]_{ii}$  of the noise on the  $i$ -th detector in the  $q$ -th frequency bin.

One may choose to fix some of these quantities (prior knowledge) and to estimate the remaining ones, either freely or under some additional parametric constraints (see section 4.1). In any case, denoting by  $\theta$  a set of free parameters defining the values of  $A_{ic}$ ,  $[C_q]_{cc}$  and  $[N_q]_{ii}$ , we obtain an estimate of  $\theta$  by minimizing a joint spectral mismatch, quantified by a weighted sum

$$\Phi(\theta) = \sum_{q=1}^Q n_q D(\hat{R}_q, R_q(\theta)). \quad (11)$$

Any sensible measure  $D(\cdot, \cdot)$  of matrix mismatch could be used to obtain a consistent estimate  $\hat{\theta}$  of the  $\theta$  parameter as  $\hat{\theta} = \arg \min_{\theta} \Phi(\theta)$ . We adopt

$$D(R_1, R_2) = \frac{1}{2} [\text{trace}(R_1 R_2^{-1}) - \log \det(R_1 R_2^{-1}) - N_d] \quad (12)$$

because then criterion (11) is, up to a constant, equal to minus the log-likelihood of the data in a simple Gaussian isotropic model (see Delabrouille, Cardoso, Patanchon (2003) for a derivation). Hence, minimizing criterion (11) is equivalent to maximizing the likelihood. This fact guarantees good performance (at least for large  $n_q$ ) when the

data do come from an isotropic random field. Also, the connection with the likelihood criterion suggests a simple optimization strategy using the EM (expectation-maximization) algorithm. In practice, minimization of the spectral mismatch (11) is achieved with the EM algorithm followed by few steps of a descent method (BFGS algorithm) to speed-up the final convergence.

#### 3.2 Error estimation

The SMICA estimator being a maximum likelihood estimator, the asymptotic variance-covariance matrix of the estimates is given, when the model holds for some value  $\theta_0$  of the parameters, by

$$\text{Cov}(\hat{\theta}) = \langle \{(\hat{\theta} - \theta_0)(\hat{\theta} - \theta_0)^t\} \rangle \approx J(\theta_0)^{-1} \quad (13)$$

where the Fisher information matrix  $J(\theta_0)$  is, in our model

$$[J(\theta_0)]_{ij} = \frac{1}{2} \sum_q n_q \text{trace} \left\{ R_q^{-1} \frac{\partial R_q}{\partial \theta_i} R_q^{-1} \frac{\partial R_q}{\partial \theta_j} \right\} \quad (14)$$

with all quantities evaluated at point  $\theta_0$ . In practice,  $J(\theta_0)$  is approximated by replacing, for each frequency bin  $q$ , matrix  $R_q$  by  $\hat{R}_q$  and matrix  $\frac{\partial R_q}{\partial \theta_i}(\theta_0)$  by  $\frac{\partial R_q}{\partial \theta_i}(\hat{\theta})$ .

Departure from stationarity<sup>3</sup> and Gaussianity does not introduce bias in parameter estimation but is likely to induce a larger estimation error than predicted by the above formula. The accuracy of the error bars prediction can be checked thanks to simulations.

The galactic and point source mask has the effect, to first order, of decreasing the effective number  $n_q$  of modes in each bin by a factor equal to the fraction of sky coverage. This is accounted for by multiplying every parameter error estimate by the inverse square root of this factor. This procedure has been validated with the help of numerous Monte-Carlo simulations.

#### 3.3 Mismatch measure

The SMICA approach includes a built-in goodness of fit: the departure of the spectral statistics  $\hat{R}_q$  from the best fit model of independent components is quantified by the divergence  $D(\hat{R}_q, R_q(\hat{\theta}))$  which should be statistically small. For a known  $N_d \times N_c$  mixing matrix, if the model of observations is correct, then  $2n_q D(\hat{R}_q, R_q(\hat{\theta}))$  is asymptotically (*i.e.* for  $n_q$  large enough) distributed as a  $\chi^2$  with  $N_d(N_d+1)/2 - (N_c + N_d)$  degrees of freedom. This value is obtained by subtracting the number of adjustable parameters per frequency bin ( $N_c$  auto-spectra plus  $N_d$  noise levels) from the  $N_d(N_d+1)/2$  degrees of freedom of a symmetric matrix. In particular:

$$\langle n_q D(\hat{R}_q, R_q(\hat{\theta})) \rangle = \frac{1}{2} \left[ \frac{N_d(N_d+1)}{2} - (N_c + N_d) \right]. \quad (15)$$

<sup>3</sup> In particular, as a consequence of WMAP scanning strategy, the noise variance per pixel on the observed maps is higher by a factor of the order of 4 around the ecliptic equator as compared to the pole regions.

### 3.4 Beam and coverage effects

We discuss the corrections needed to account for beam and coverage effects.

In first approximation, if a mask covers a fraction  $\alpha$  of the sky, an effective number  $\alpha n_q$  should be used in place of  $n_q$ . However, since masking also introduces mode coupling, a better approximation is desired. We follow the MASTER formalism developed by Hivon et al. (2002). The idea is as follows: let  $s(\theta, \phi)$  be an isotropic Gaussian random field with harmonic spectrum  $c(\ell)$ , of which only a masked version  $\tilde{s}(\theta, \phi) = w(\theta, \phi)s(\theta, \phi)$  is observed. Denoting  $\tilde{s}(\ell, m)$  the harmonic coefficients of  $\tilde{s}(\theta, \phi)$ , we have

$$\frac{1}{2\ell + 1} \sum_{m=-\ell}^{m=\ell} \langle |\tilde{s}(\ell, m)|^2 \rangle = \sum_{\ell'} M_{\ell\ell'} c(\ell') \quad (16)$$

where the coefficients  $M_{\ell\ell'}$  depend only on the mask (and thus can be computed independently of the data). Hence, if  $M_{\ell\ell'}$  is known, so is the bias introduced by the mask on the harmonic spectra.

In practice, we proceed as follows. In a first step, the input maps are masked, transformed to the spherical harmonic domain and brought to a common resolution (see section 2.1). Next, bin-averaged empirical spectral matrices are computed according to eq. (8) and a model of independent components is adjusted to them by minimizing (11). The resulting bin-averaged harmonic spectra of each component is then corrected by inverting the bin-averaged version of relation (16). This last stage also incorporates the correction of the common beam pattern.

### 3.5 Component map separation

Ideally, component maps would be estimated by applying a Wiener filter  $W = [A^t N^{-1} A + C^{-1}]^{-1} A^t N^{-1}$  to the observations. This solution maximizes the signal to noise ratio on each individual component map (here noise means detector noise plus other astrophysical component emissions). In the limiting case where noise is small as compared to component signals,  $C^{-1}$  is negligible and the Wiener filter yields unbiased (in the sense that  $WA = I$ ) estimates of the maps. In poor signal to noise regimes, the signal is attenuated to suppress noise contamination in the reconstructed maps.

In practice, the Wiener filter is applied in the frequency domain, using estimated values  $\hat{A}$ ,  $\hat{N}$  and  $\hat{C}$  of the parameters. The harmonic coefficients of the estimated components are obtained as

$$\hat{s}(\ell, m) = [\hat{A}^t \hat{N}_q^{-1} \hat{A} + \hat{C}_q^{-1}]^{-1} \hat{A}^t \hat{N}_q^{-1} x(\ell, m) \quad (17)$$

when  $\ell_{\min}(q) \leq \ell \leq \ell_{\max}(q)$ .

## 4 APPLICATION & RESULTS

We now present a SMICA analysis of WMAP data. The two data sets described in section 2.1 (map set I corresponding to sky regions outside of Kp2 mask, and map set II corresponding to galactic latitudes higher than 40 degrees, with the strongest point sources masked in both cases) are used for two independent analyses.

### 4.1 Choice of parameters for SMICA

In a preliminary analysis, we have looked for the total number of components required by the map set I without imposing constraints neither on the amplitude of the estimated components nor on their spatial power spectra. In this totally blind analysis, we found two significant components. The first component, dominant in all channels, is clearly identified as CMB. The second, weaker by several orders of magnitude and essentially significant in the Q band (it is detected to a lesser extent in the V and W bands) is thought to be a mixture of residual galactic emissions and unresolved point sources. These last two processes cannot be reliably separated without introducing additional constraints because of nearly proportional mixing matrix columns (both components dominate in the Q band and are almost negligible in the others).

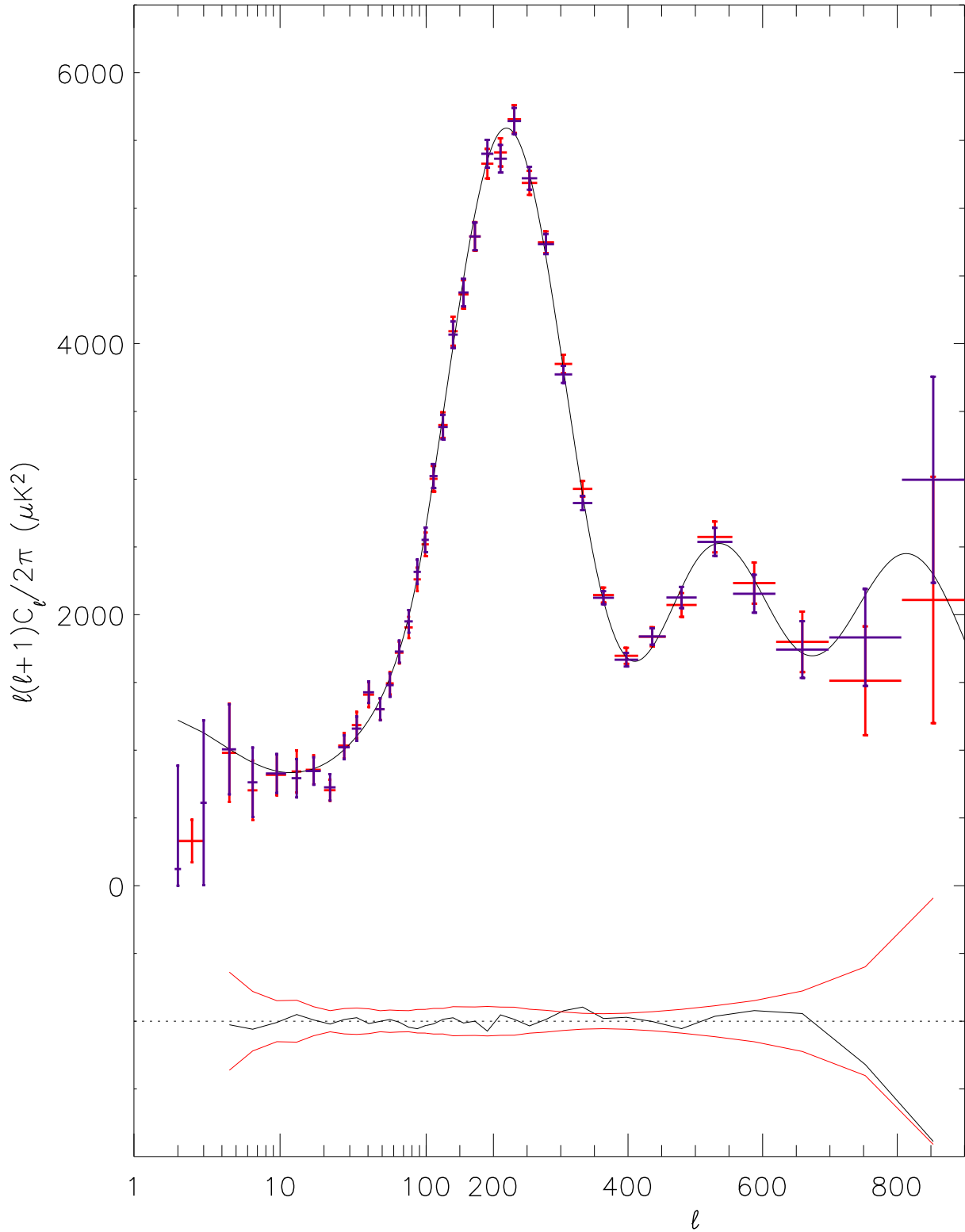
In order to differentiate between residual galactic emission and point sources, we need to introduce some physical knowledge in the form of constraints on the system. Therefore, in most of the subsequent analysis, unless explicitly stated otherwise, we adjust a model with three components, one of them being strongly constrained to capture point source contributions as follows. The emission spectrum of point sources is well described, at WMAP frequencies, by a power law with a spectral index  $\beta \approx -2$  (section 2.3) and their spatial power spectrum is expected to be almost flat since the effect of clustering is negligible in practice at radio frequencies (González-Nuevo et al. 2004). Hence, for one component, meant to be residual point source emission, we fix the mixing parameters (the column of the mixing matrix) to  $A_{i,PS} = (\nu_i/\nu_0)^{-2}$  in RJ temperature units, and we constrain the harmonic power spectrum to be flat. Only one parameter, its amplitude, is left free to match the contribution of this component.

In summary, we match spectral matrices with three components. For two of them, meant to be CMB anisotropies and residual galactic emission, no constraint on parameters are enforced (both the mixing parameters and the power spectra are determined exclusively from the data). The last component is constrained to have the emission law and spectral shape of point sources; only its amplitude can be adjusted (but see figure 7 and the related comments). Finally, regarding noise, the average noise power is freely estimated in each map and each frequency bin.

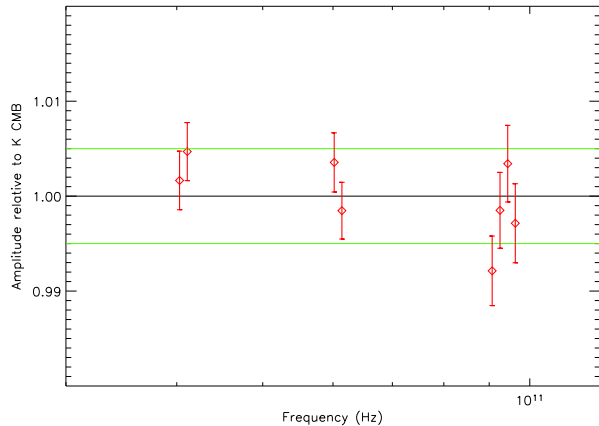
### 4.2 CMB anisotropies

Figure 1 shows the estimated CMB power spectrum after correcting for partial coverage and beam and pixel transfer functions. It displays a peak around  $\ell = 200$  (first acoustic peak) and a second peak around  $\ell = 550$ , both compatible with the measurement announced by the WMAP team.

SMICA and WMAP team power spectrum estimations show an excellent agreement for most multipoles. For multipoles between  $\ell = 2$  and  $\ell = 290$  the difference between the two power spectra is much smaller than error bars (except for bins centered on  $\ell = 190$  and  $\ell = 210$  where the difference is of the order of the error bars), but is larger than statistical errors after removing cosmic variance contribution. This can be explained (at least partially) by the small differences in the sky coverage due to the apodisation procedure we apply



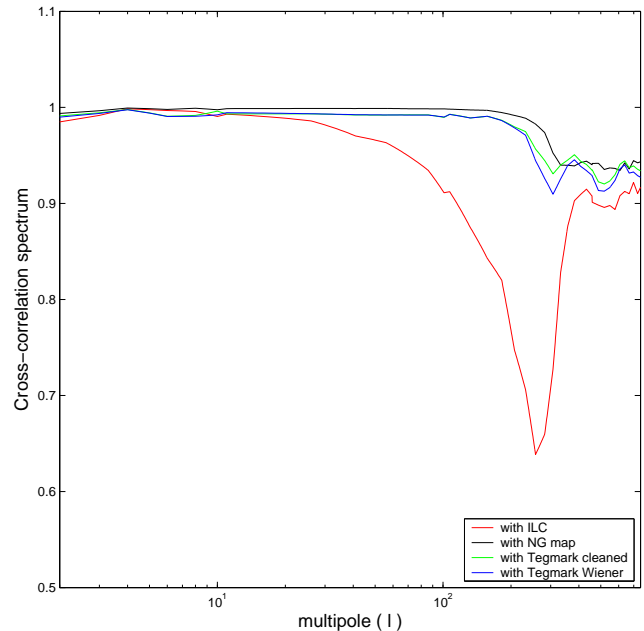
**Figure 1.** The CMB spatial power spectrum measured with SMICA (in red) as compared to the published WMAP 1 year spectrum (in blue). The error bars from SMICA are computed from the Fisher information matrix using the parameters at convergence (and not the parameters of the model). This explains the small error bar on the first bin of the SMICA estimate. We also plot the difference of the power spectra for better comparison. The red curves correspond to  $\pm 1\sigma$  error bars on the power spectrum obtained with SMICA.



**Figure 2.** Measured amplitude of CMB fluctuations in each detector (in red) relative to temperature fluctuation units as given by the calibration on the dipole. The amplitude of the fluctuations are normalized to 1 on average. Data points at the same frequency have been slightly offset in abscissa for readability. Blue lines delimit calibration 1 sigma errors provided by the WMAP team. The errors on estimated mixing parameters are statistical errors computed from the Fisher information matrix at convergence. In order to provide an error bar on every CMB mixing parameter, errors are not marginalized on CMB power spectrum estimate (there is a degeneracy between power spectrum amplitude and mixing parameters normalization).

on the maps. For larger multipoles, the two estimates show somewhat larger differences which may be due, in part, to the two different weighting schemes used by the two methods for  $\ell > 200$ . For SMICA, no weighting of the pixels depending on the noise variance per pixel is applied prior to the analysis. On the contrary, the WMAP team applies different weighting schemes for  $\ell > 200$  (a weighting proportional to  $1/\text{noise}^2$  for  $\ell > 450$  and a transition weighting for  $200 < \ell < 450$ ). Hence, discrepancies between the two estimates are expected to be larger for  $\ell > 200$  since the two data sets are not quite identical. This may account for the small observed differences. We note in the passing that the small dip at the top of the first acoustic peak in the WMAP team estimate has disappeared in the SMICA estimate.

Figure 2 shows the estimated amplitude of CMB anisotropies for all the observation channels, as given by the CMB column of the estimated mixing matrix  $\hat{A}$ . We find an emission law compatible with the expected derivative of a blackbody, to excellent accuracy. A fit of the form  $\nu^\alpha$  gives  $\alpha = -0.0067 \pm 0.0058$  compatible with 0 at about 1.15 sigma. Refined calibration and systematics testing, as well as the second year data, will reduce the error bar and clarify the significance of a possible deviation from the expected blackbody derivative. Note that, given the error bars, *the accuracy of the measurement of the CMB emission law is limited by detector calibration uncertainty rather than intrinsic statistical errors!* The present measurement shows that the emission law of the anisotropies is the same as that of the dipole, which is itself known (under the assumption that it is essentially due to a kinetic effect) to be the derivative with respect to temperature of the CMB blackbody emission measured with FIRAS.



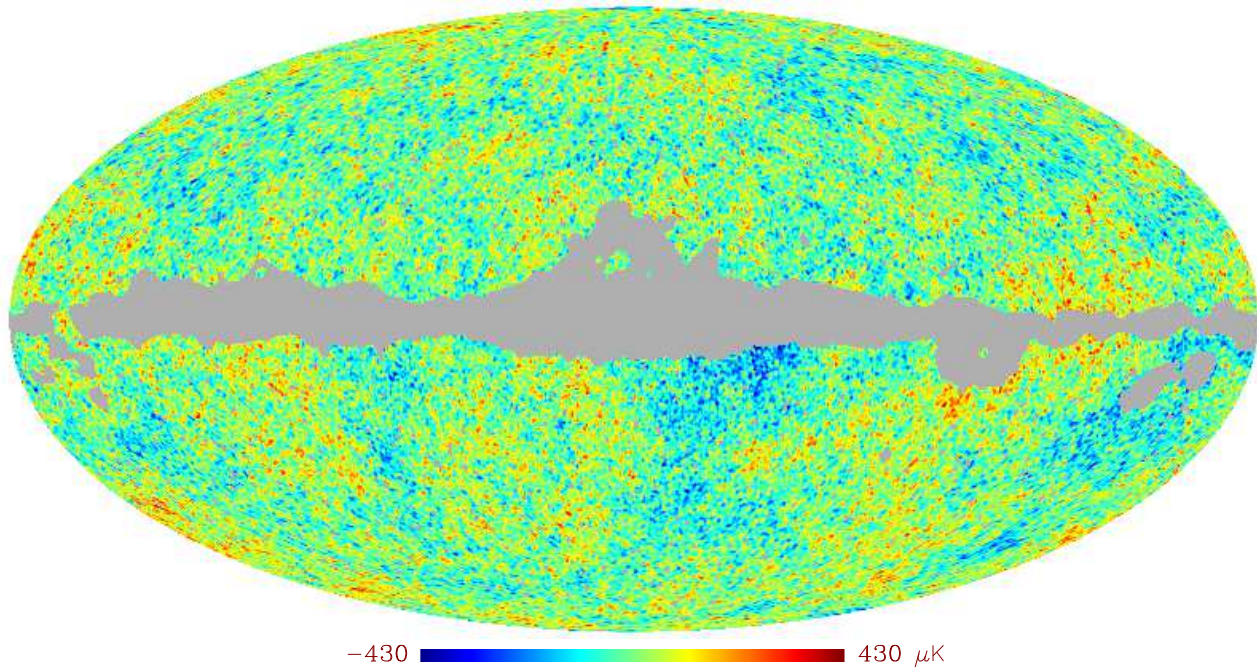
**Figure 4.** Cross-correlation spectra between our CMB map with other available CMB maps from the WMAP data: the ILC map published by the WMAP team (Bennett et al. 2003b), the combined map used for non-Gaussianity studies (e.g., Komatsu et al. 2003) and the two maps (*cleaned* and *Wiener filter*) obtained by Tegmark et al. (2003).

Figure 3 displays a reconstruction of the CMB anisotropy map by Wiener filtering (equation 17) using the parameters estimated with SMICA. The now familiar CMB anisotropy pattern is clearly visible.

We have compared our recovered CMB map with other available CMB maps from WMAP: the Internal Linear Combination (ILC) map published by the WMAP team (Bennett et al. 2003b), the combined map used for non-Gaussianity analysis (e.g., Komatsu et al. (2003)) and the two maps (*cleaned* and *Wiener filter*) obtained by Tegmark (Tegmark et al. 2003).

As seen on figure 4, we find very high correlation ( $\approx 99\%$ ) with the two maps proposed by Tegmark as well as with the map used for non-Gaussianity studies up to  $\ell \approx 200$ . The correlation slightly decreases down to  $\approx 95\%$  for multipoles larger than 200 (see Figure 4). The cross-correlation with the ILC map is also around of 99%, but only up to multipoles  $\ell \approx 20$ . For smaller scales, the correlation with the ILC map decreases down to  $\approx 60\%$  at  $\ell \approx 200$  and then it increases up to  $\approx 90\%$  at the smallest scales. The fact that the correlation with the ILC is smaller than with the other CMB maps is not surprising since, as explained by the WMAP team, the ILC was developed for foreground analyses and it is far for being the best CMB reconstruction (Bennett et al. 2003b).

We have also tested possible contamination caused by unsubtracted foreground emissions by cross-correlating our CMB reconstruction with templates of different Galactic emissions (synchrotron, thermal dust and free-free). We find no significant contamination, since the correlation level is below the dispersion of the casual correlations between those templates and CMB Gaussian simulations (5 – 10%).



**Figure 3.** Map of CMB fluctuations obtained after Wiener filtering of the data using parameters estimated with SMICA.

detector	Q1	Q2	V1	V2	W1	W2	W3	W4
ampl. (K/K)	1	0.85	0.04	0.02	-0.13	-0.27	-0.22	-0.16
error (K/K)	0	0.08	0.07	0.07	0.08	0.09	0.09	0.09

**Table 1.** Estimated relative amplitude of the second component in each of the observed map in Rayleigh-Jeans (RJ) temperature units and associated errors. The normalization of parameters is fixed with respect to Q1 map. Error on parameters are correlated at the 20% level.

### 4.3 Residual galactic emission

Table 1 gives the emission law (the column of the mixing matrix) estimated for the second component in the map set I. Parameters are rescaled to normalize to unity in the Q1 band (where the component dominates) in order to fix the degeneracy between mixing parameter normalization and power spectrum amplitude. Although much lower than the CMB, this second component is clearly detected in the Q band (at about 10 standard deviations). Its mixing parameters are compatible with 0 in V-bands, and are systematically negative and detected at about two standard deviations on average in each individual map of the W-bands except W1. Mixing parameters for radiometers observing at the same frequency are compatible with a constant value, as expected for an astrophysical component. The amplitude of the component is at least 10 times larger in the Q band than in the V band (in Rayleigh Jeans (RJ) temperature units), and is larger in absolute value in the W band than in the V band. This behavior is not *a priori* excluded if the component orig-

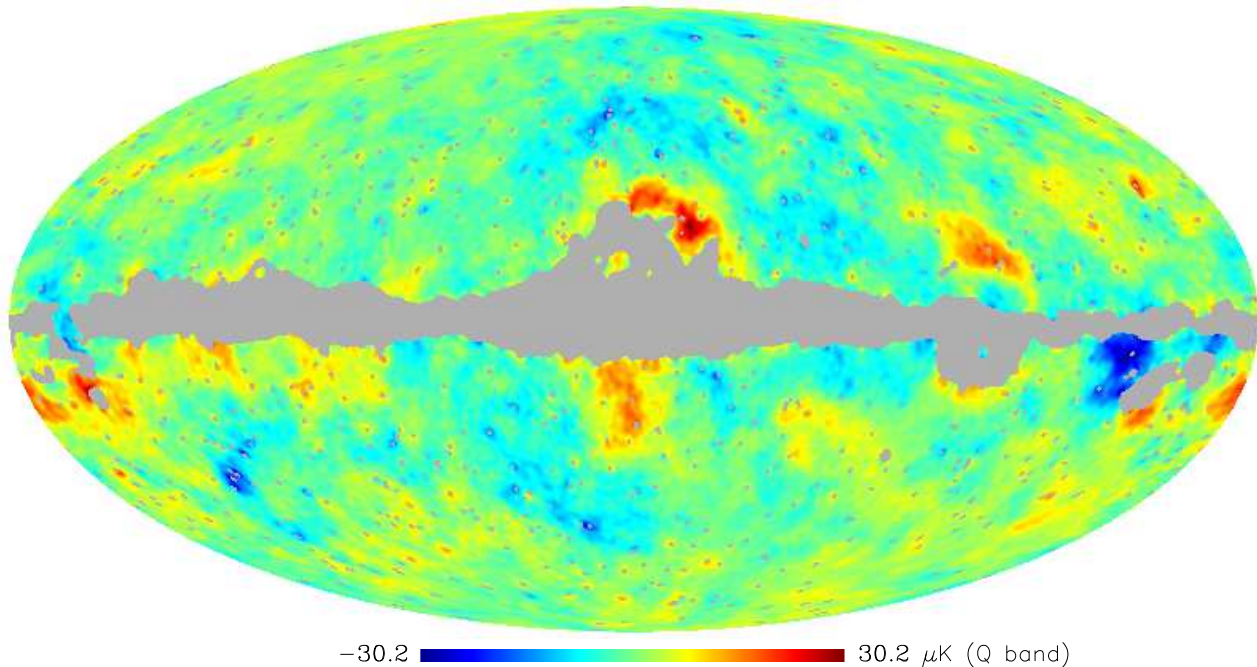
inate from residual galactic emission (mainly synchrotron and dust correlated emission) after galactic foreground removing operation by the WMAP team. In that case, mixing parameters of two different frequencies may have opposite signs depending on the sign of the error on the parameters of the template fit.

Figure 5 shows the map of the residual component obtained by Wiener filtering using estimated parameters. We can notice a bright structure close to the galactic center at the edges of the galactic mask which we identify as a residue from foreground subtraction in the *Ophiuchus complex*. Other residual structures associated to the *North polar spur*, the *Gum nebula*, the *Orion-Eridanus bubble* and the *Taurus* region can also be identified, suggesting that the emission of these regions does not perfectly match the model used by WMAP team.

We have found a significant correlation ( $\approx 40\%$ ) between our second component and the WMAP synchrotron emission estimation at the Q band (using MEM, see Bennett et al. 2003b), which supports the Galactic origin of our second component.

As can be seen from the Wiener map (and as expected for galactic emission), the component looks very non-stationary over the sky. As the stationarity of components is assumed in our model, errors on mixing parameters probably are somewhat underestimated but we do not expect this to change our interpretation.

Figure 6 shows the estimated power spectra of the second component in both map sets I and II. For the estimation with the map set II, we have fixed the mixing parameters



**Figure 5.** Map of the residual component as “seen” in the Q-band, obtained by Wiener filtering using estimated parameters.

of the residual component, as well as the amplitude of point source power spectrum to the results obtained in the map set I. This allows to compare the two power spectra estimates of a component with a fixed effective emission law. The estimated power spectrum of the residual component in map set I is measured with high significance for multipoles between  $\ell = 2$  and  $\ell \simeq 150$  and form a plateau ( $\ell^2 c(\ell) \approx \text{const}$ ) with an amplitude  $\approx 10 - 12 \mu\text{K}^2$  in the Q-band. For higher multipoles, the beam transfer function of Q-band detectors strongly suppresses the signal, and the sensitivity is not sufficient to allow an accurate measurement of the component. Nevertheless, the last three bins show weak incompatibilities with 0 at 1.5-2 sigma. Errors on those three parameters are strongly correlated (to  $\approx 50\%$  due to the anti-correlation of those parameters with the amplitude of point sources emission), so there is not clear evidence of detection at high spatial frequencies.

The power of the residual component for angular scales larger than 1-2 degrees is clearly reduced at galactic latitude higher than 40 degrees. It remains marginally detectable even though it is reduced by a factor greater than 4 for  $\ell$  between about 10 and 30.

We find that the power of the remaining galactic foreground contamination in WMAP maps (outside of Kp2 mask) is about 1% of the CMB anisotropy variance at large angular scales ( $\ell < 100$ ) at 41 GHz. This result is in agreement with the WMAP team estimate, based on correlation measurement using external foreground templates (Bennett et al. 2003b). The power of the residual compo-

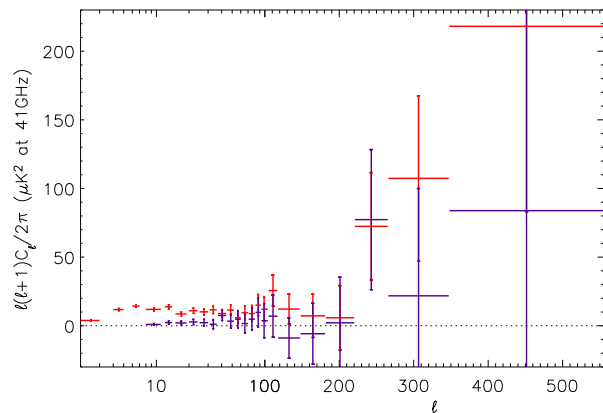


**Figure 6.** Estimated power spectrum of the second component from SMICA analysis in map set I (red ink) and comparison with the power spectrum estimated at galactic latitudes higher than 40 degrees (map set II, blue ink). Power spectra amplitudes are rescaled on the Q-band. No positivity constraints are enforced for parameter estimates, making it easy to check their compatibility with 0. Cosmic variance, naturally included in error bar computation from the Fisher information matrix, has been removed afterwards from the error estimates. Estimated power spectra are re-binned for readability. Due to the lower sky coverage fraction for map set II (30%), the large angular scales are poorly constrained. We then restrained the analysis to multipoles  $\ell > 10$  only.

ment is less than 0.2 % of the CMB variance at 61 and 94 GHz.

#### 4.4 Unresolved point source emissions

In our analysis, the third component is rigidly constrained: as described above (sec. 4.1), the mixing parameters and the shape of the power spectrum are fixed to values expected for unresolved point sources emission, leaving only the overall amplitude to be determined by spectral matching. We find  $C_{\text{PS}}(\ell) = (9.2 \pm 5.0) \times 10^{-3} \mu\text{K}^2$  at 41 GHz. This value is marginally compatible with the WMAP team estimate (see Komatsu et al. (2003) for a discussion for the expected contribution of unresolved point sources to the CMB power spectrum, for different masks and flux limits) and model predictions (Argüeso et al. 2003):  $15.5 \pm 1.7 \times 10^{-3} \mu\text{K}^2$ .

The large error bar on our estimate is due to the difficulty of discriminating components with similar spectral characteristics. In this experiment, the residual galactic component and the point source component have similar effective emission laws (mixing matrix elements) and both components dominate in the Q-band and can not be accurately estimated in V and W bands. So, some power at high spatial frequency can be exchanged between the second and the third components without modifying dramatically the likelihood of the model.

We further investigate the distribution of the third component by performing two additional spectral matches on map set II. Neglecting residual galactic emissions (we have seen in previous section that residual galactic emission is clearly reduced at high galactic latitude), we now fit a two-component model (as opposed to previous matches, build with three components) with two different constraint set. In a first match, all parameters related to point sources emission law and power spectra are fixed, except the amplitude which is fitted. We find the amplitude of the power spectrum to be:  $C_{\text{PS}}(\ell) = (11.3 \pm 3.5) \times 10^{-3} \mu\text{K}^2$  at 41 GHz, in better agreement with the value already reported of  $15.5 \pm 1.7 \times 10^{-3} \mu\text{K}^2$ . In a second match, we relax all constraints on the shape of the power spectrum to obtain estimates of the power spectrum in every multipole bin. The resulting power spectrum of unresolved point sources is displayed in figure 7. Parameters are clearly incompatible with 0 for most of the multipoles (assuming *a priori* a smooth power spectrum). A good compatibility with the model  $C_{\text{PS}}(\ell) = 11.3 \times 10^{-3} \mu\text{K}^2$  (41 GHz) is observed. If we re-adjust the model of the power spectrum to the estimated parameters using a simple  $\chi^2$  we obtain a similar value for the amplitude. Nevertheless, a weak excess of power can be seen for the lowest multipoles ( $\ell < 50$ ) possibly due to a remaining galactic contamination at high galactic latitudes.

#### 4.5 Goodness of fit

In this section, we briefly examine the fit of the best models to the data across frequency bins by plotting the weighted mismatch  $n_q D(\hat{R}_q, R_q(\hat{\theta}))$  against the bin index  $q$ . If the model of independent stationary component holds, the expected value of this measure of mismatch is given, for  $n_q$  large enough, by eq. (15). In our plots, however, we use

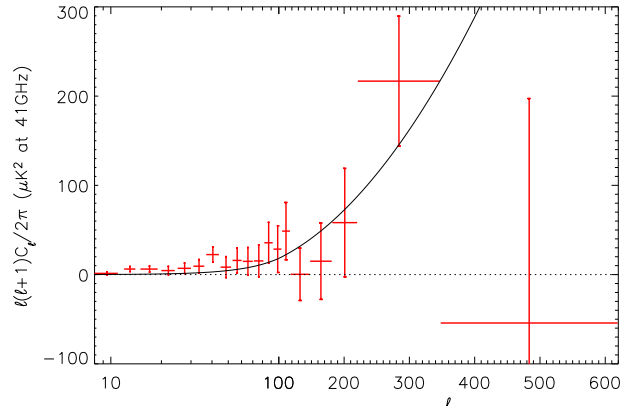


**Figure 7.** Power spectrum of unresolved point sources emission estimated with SMICA assuming two components in the map set II (red). Mixing parameters of point source emission have been fixed for the analysis. No constraints of positivity is given for parameter estimates allowing to check easily their compatibility with 0. Cosmic variance has been removed afterwards from the error estimates. The black curve corresponds to the model of point source power spectrum  $C_{\text{PS}}(\ell) = \text{const}$  with an amplitude estimated from the semi-blind approach of  $11.3 \times 10^{-3} \mu\text{K}^2$  (see text for details).

Monte-Carlo simulations to have an estimate of the distribution of the mismatch valid even in the non asymptotic regime. We report goodness of fit of adjusted models in two cases: a one-component model and a three-component model.

Figure 8 shows that the one-component model is clearly incompatible with the data for  $\ell < 60$ . It also shows that the fit obtained with three components is very satisfactory for most of the multipoles although small discrepancies remain, in particular for  $\ell$  between 10 and 25. We interpret this as a clear indication that residual galactic emission are present in the data at low spatial frequency.

We can investigate the origin of the remaining discrepancies by looking at the spectral mismatch between *pairs* of detectors. Figures 9 shows the goodness of fit between the individual pair of detectors (Q1,Q2), assuming either one or three components. The misfit for the one-component model is now even more obvious (as compared to the global mismatch involving all detectors), as expected since the Q band is where the galactic residual dominates.

As the second component is detected in the W channel as well, we also looked at the fit of one-component and three-component models for all W detectors together and for the set of W2, W3 and W4 (discarding W1). For both figures, the goodness of fit is significantly better for three components than for a unique component for low multipoles.

A significant excess remains, which is probably due to fine departure of the residual galactic emission from the single template assumption. Figure 10, however, rather point to remaining systematics in the W1 channels since the mismatch is significantly reduced when excluding the W1 detector.

This incompatibility, however, is small enough so that

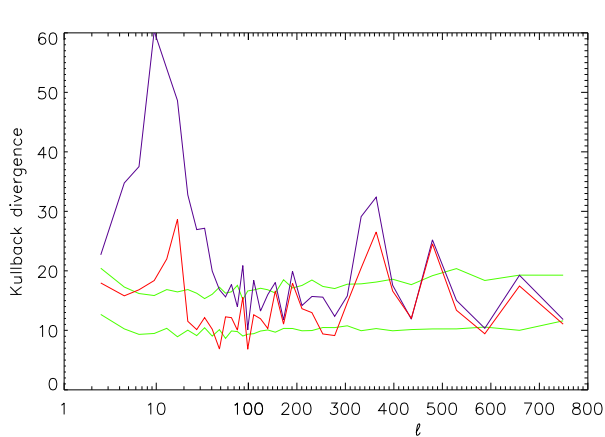


**Figure 8.** Spectral mismatch for map set I, with three components (red) and 1 component (blue). The green curves are the boundaries of the 68% goodness of fit interval estimated using simulations. For three components, the fit is very satisfactory for most of the spatial frequencies (see text).

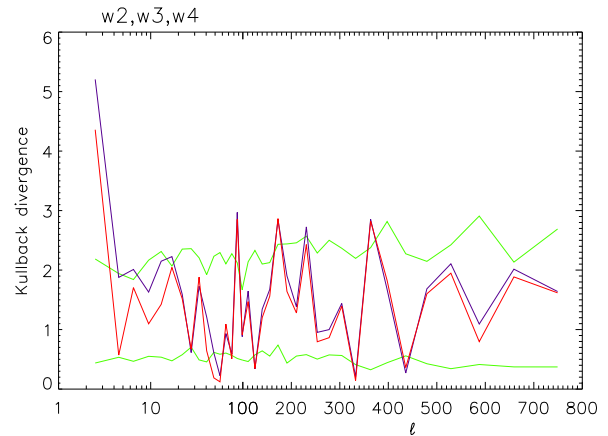
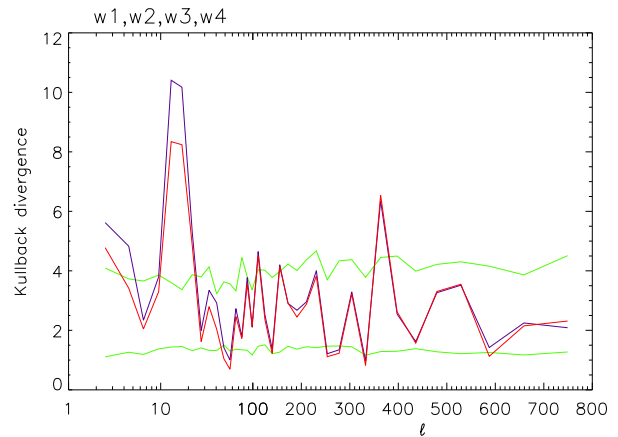


**Figure 10.** Spectral mismatch with three components (red) and one component (blue). Top: mismatch for all four W band detectors; bottom: for three last W band detectors (W1 excluded).

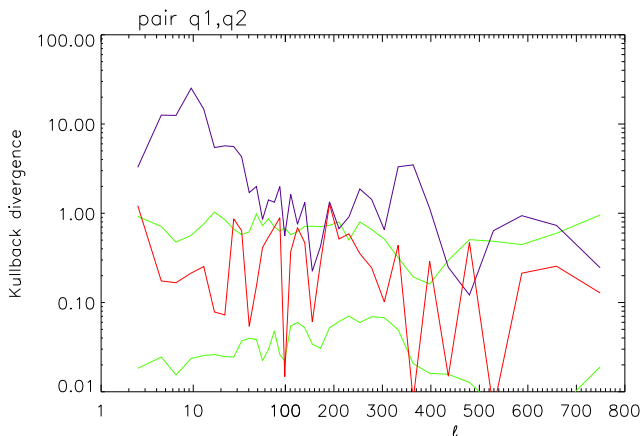


**Figure 9.** Spectral mismatch for the detector pair (Q1,Q2) only, with three components (red) and one component (blue). The green curves are the boundaries of the 68% interval estimated using simulations. Note the logarithmic scale and thus the very significant reduction of the mismatch when three components are considered.

the CMB power spectrum is not affected because the errors for the lowest multipoles are dominated by cosmic variance.

## 5 CONCLUSIONS

We have performed a blind multi-component analysis of the first year WMAP data. We used the eight foreground-cleaned high frequency maps (Q1 to W4) provided by the WMAP collaboration. Our analysis uses SMICA, a maximum likelihood spectral matching method. Three significant astrophysical components

- the CMB anisotropies
- a residual galactic emission
- unresolved point source emissions

are jointly characterized in the foreground cleaned maps after masking the strongest point sources and the galactic plane using Kp2 mask. No significant thermal SZ emission is found with the present study, in agreement with the WMAP team (Bennett et al. 2003b) and Huffenberger, Seljak, Makarov (2004).

Blind analysis allows us to estimate the power spectrum of CMB anisotropies as well as their amplitude across frequency channels confirming their cosmological nature. Our power spectrum estimate is in excellent agreement with the WMAP team estimate. We show that the measured emission law of CMB anisotropies at WMAP frequencies is compatible with the derivative of a blackbody, as expected for temperature fluctuations. The statistical errors on parameters related to the amplitude of the anisotropies are about 0.3%, and are smaller than calibration errors (0.5%) on dipole modulation. Conversely, if CMB anisotropies are assumed to be pure temperature fluctuations, then the estimation of CMB amplitude across channels provides a relative calibration across frequency bands at a better precision than dipole calibration.

The second estimated component, corresponding to a weak residual galactic emission, is mainly concentrated in Q-band maps outside of the Kp2 mask. We believe that this component results mainly from spatial variations of

the difference between Haslam map (used as a synchrotron template for the subtraction) and synchrotron emission at WMAP frequencies. This component is weak compared to CMB anisotropies. The estimated power spectrum is about  $\ell(\ell + 1)C(\ell)/2\pi \approx 10 - 12\mu K^2$  for  $\ell < 100$  in Q band and less than  $2\mu K^2$  in V and W band. Those estimates are compatible with WMAP team estimates of foreground contamination. Finally, much of the power from this residual large scale component disappears for galactic latitude higher than 40 degrees.

The third component corresponds to residual point sources emission. By fixing the parameters related to the emission law of point sources (we assume  $(\nu/\nu_0)^{-2}$ ) and to the power spectrum (flat power spectrum), we estimate the amplitude of unresolved point source power spectrum. We find at high galactic latitude:  $C(\ell) = (11.3 \pm 3.7) \times 10^{-3} \mu K^2$  at 41 GHz compatible with the WMAP team estimation. We also provide an estimate of the power spectrum of point sources at high galactic latitude.

The goodness of fit of the 3-component model is excellent, except for a very small discrepancy around  $\ell \approx 20$  which is likely to be attributed to a systematic in W1. This inconsistency has no impact on the CMB power spectrum estimate (because errors are dominated by cosmic variance), but could affect the estimates of weak components in data.

## 6 ACKNOWLEDGMENTS

This work was supported by the Canadian Natural Sciences and Engineering Research Council and by the French ministry of research. GP would like to thank Mark Halpern for useful discussions. We acknowledge the use of the Legacy Archive for Microwave Background data analysis (LAMBDA). Some results of this paper have been derived using the HEALPix (Górski, Hivon, Wandelt 1998) package. We acknowledge the use of the software package CMBFAST (<http://www.cmbfast.org>) developed by U. Seljak and M. Zaldarriaga.

## REFERENCES

- Argüeso F., González-Nuevo J., Toffolatti L. , *The Astrophysical Journal*, **598** (2003), 86–96, Contributions of Point Extragalactic Sources to the Cosmic Microwave Background Bispectrum
- Bennett C. L., Halpern M., Hinshaw G., Jarosik N., Kogut A., Limon M., Meyer S. S., Page L., Spergel D. N., Tucker G. S., Wollack E., Wright E. L., Barnes C., Greason M. R., Hill R. S., Komatsu E., Nolte M. R., Odegard N., Peiris H. V., Verde L., Weiland J. L., *The Astrophysical Journal Suppl.* **148** (2003) 1–27, First-Year Wilkinson Microwave Anisotropy Probe (WMAP) Observations: Preliminary Maps and Basic Results
- Bennett C. L., Hill R. S., Hinshaw G., Nolte M. R., Odegard N., Page L., Spergel D. N., Weiland J. L., Wright E. L., Halpern M., Jarosik N., Kogut A., Limon M., Meyer S. S., Tucker G. S., Wollack E., *The Astrophysical Journal Suppl.* **148** (2003) 97–117, First-Year Wilkinson Microwave Anisotropy Probe (WMAP) Observations: Foreground Emission
- Bouchet F.R., Gispert R., *New Astronomy* **4** (1999) 443, Foregrounds and CMB experiments I. Semi-analytical estimates of contamination
- Cardoso J.-F., Snoussi H., Delabrouille J., Patanchon G., EUSIPCO02 conference proceedings **1** (2002) 561–564, Blind separation of noisy Gaussian stationary sources. Application to cosmic microwave background imaging
- Delabrouille J., Cardoso J.-F., Patanchon G., *Monthly Notices of the RAS* **346** (2003) 1089, Multi-Detector Multi-Component spectral matching and applications for CMB data analysis
- Finkbeiner D. P., Davis M., Schlegel D. J., *The Astrophysical Journal* **524** (1999) 867–886, Extrapolation of Galactic Dust Emission at 100 Microns to Cosmic Microwave Background Radiation Frequencies Using FIRAS
- Finkbeiner D. P., *The Astrophysical Journal Suppl. Series* **146** (2003) 407–415, A Full-Sky H $\alpha$  Template for Microwave Foreground Prediction
- Fixsen D.J., *The Astrophysical Journal Letter* **594** (2003) 67–70, The Spectrum of the Cosmic Microwave Background Anisotropy from the Combined COBE FIRAS and WMAP Observations
- González-Nuevo J., Toffolatti L. , Argüeso F., preprint, astro-ph/0405553, EPSS-2D: a fast computer code for simulating all-sky maps of clustered extragalactic point sources
- Górski K.M., Hivon E., Wandelt B.D., in *Proceedings of the MPA/ESO Cosmology Conference, Evolution of Large-Scale Structure*, eds. A.J. Banday, R.S. Sheth and L. Da Costa, Garching (1998). Analysis issues for large cmb data sets
- Haslam C. G. T., Stoffel H., Salter C. J., Wilson W. E., *Astronomy and Astrophysics Suppl. Series* **47** (1982) 1, A 408 MHz all-sky continuum survey. II - The atlas of contour maps
- Hinshaw G., Spergel D. N., Verde L., Hill R. S., Meyer S. S., Barnes C., Bennett C. L., Halpern M., Jarosik N., Kogut A., Komatsu E., Limon M., Page L., Tucker G. S., Weiland J. L., Wollack E., Wright E. L., *The Astrophysical Journal Suppl.* **148** (2003) 135–159, First-Year Wilkinson Microwave Anisotropy Probe (WMAP) Observations: The Angular Power Spectrum
- Hivon E., Górski K.M., Netterfield C.B., Crill B.P., Prunet S., Hansen F., *The Astrophysical Journal* **567** (2002) 2–17, MASTER of the Cosmic Microwave Background Anisotropy Power Spectrum: A Fast Method for Statistical Analysis of Large and Complex Cosmic Microwave Background Data Sets
- Huffenberger K.M., Seljak U., Makarov A., astro-ph/0404545
- Jungman G., Kamionkowski M., Kosowsky A., Spergel D.N., *Phys. Rev. D* **54** (1996) 1332, Cosmological-parameter determination with microwave background maps
- Komatsu E., Kogut A., Nolte M. R., Bennett C. L., Halpern M., Hinshaw G., Jarosik N., Limon M. Meyer S. S., Page L., Spergel D. N., Tucker G. S., Verde L., Wollack E., Wright E. L., *The Astrophysical Journal Suppl.* **148** (2003) 119–134, First-Year Wilkinson Microwave Anisotropy Probe (WMAP) Observations: Tests of Gaussianity
- Patanchon G., Snoussi H., Cardoso J.-F., Delabrouille J.,

- PSIP03 proceedings **1** (2003) 17–20, Component separation for Cosmic Microwave Background data: a blind approach based on spectral diversity
- Smoot G. F., Bennett C. L., Kogut A., Wright E. L., Aymon J., Boggess N. W., Cheng E. S., de Amici G., Gulkis S., Hauser M. G., Hinshaw G., Jackson P. D., Janssen M., Kaita E., Kelsall T., Keegstra P., Lineweaver C., Loewenstein K., Lubin P., Mather J., Meyer S. S. Moseley S. H. Murdock T. Rokke L. Silverberg R. F. Tenorio L. Weiss R. Wilkinson D. T, *ApJL* **396** (1992) L1, Structure in the COBE differential microwave radiometer first-year maps
- Schlegel D. J., Finkbeiner D. P., Davis M., *The Astrophysical Journal* **500** (1998) 525, Maps of Dust Infrared Emission for Use in Estimation of Reddening and Cosmic Microwave Background Radiation Foregrounds
- Spergel D. N., Verde L., Peiris H. V., Komatsu E., Nolte M. R., Bennett C. L., Halpern M., Hinshaw G., Jarosik N., Kogut A., Limon M., Meyer S. S., Page L., Tucker G. S., Weiland J. L., Wollack E., Wright E. L., *The Astrophysical Journal Suppl.* **148** (2003) 175–194, First-Year Wilkinson Microwave Anisotropy Probe (WMAP) Observations: Determination of Cosmological Parameters
- Tegmark M., de Oliveira-Costa A., Hamilton A., 2003, *PRD*, **68**, 123523, High resolution foreground cleaned CMB map from WMAP
- Toffolatti L., Argueso Gomez F., de Zotti G., Mazzei P., Franceschini A., Danese L., Burigana C., *Monthly Notices of the RAS* **297** (1998) 117, Extragalactic source counts and contributions to the anisotropies of the cosmic microwave background: predictions for the Planck Surveyor mission
- Zaldarriaga M., Seljak U., 2000, *The Astrophysical Journal Supplement Series*, **129**, 431, CMBFAST for Spatially Closed Universes